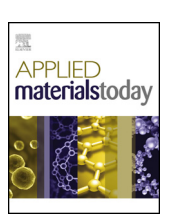
FISEVIER

Contents lists available at ScienceDirect

# **Applied Materials Today**

journal homepage: www.elsevier.com/locate/apmt



# Large-area nanostructured surfaces with tunable zeta potentials

Aktaruzzaman Al Hossain<sup>a</sup>, Mengying Yang<sup>b</sup>, Antonio Checco<sup>a</sup>, Gregory Doerk<sup>d</sup>, Carlos E. Colosqui<sup>a,c,\*</sup>

- <sup>a</sup> Department of Mechanical Engineering, Stony Brook University, Stony Brook, NY 11794, USA
- <sup>b</sup> Department of Chemistry, Stony Brook University, Stony Brook, NY 11794, USA
- <sup>c</sup> Department of Applied Mathematics & Statistics, Stony Brook University, Stony Brook, NY 11794, USA
- <sup>d</sup> Center for Functional Nanomaterials, Brookhaven National Laboratory, Upton, NY 11973, USA

#### ARTICLE INFO

Article history:
Received 3 September 2019
Received in revised form 1 December 2019
Accepted 27 December 2019

Keywords: Nanostructured surfaces Block-copolymer self-assembly Zeta potential

#### ABSTRACT

Through a refined fabrication protocol based on block-copolymer self-assembly we synthesize nanostructured surfaces with conical nanopillars of different height (60, 120, and 200 nm) in hexagonal arrays with uniform spacing ( $\sim$ 50 nm) over large areas (> cm²). While the nanostructured surfaces fabricated on silicon substrates display superhydrophilic behavior, superhydrophobic properties are attained by coating with octadecyltrichlorosilane (OTS). Negative zeta potentials for all the studied surfaces are reported by electrokinetic flow measurements with aqueous KCl solutions at different concentrations (1 and 10 mM) and pH values between 4 and 8. While the surface nanostructure reduces the zeta potential magnitude, the hydrophobic OTS coating enhances it. Experimental results can be accounted for by a site-dissociation model for the surface charge density. The reported wetting properties and zeta potential tunability makes the studied surfaces particularly relevant for applications such as energy conversion and storage, membrane-based water treatment and molecular separation.

© 2019 Published by Elsevier Ltd.

# 1. Introduction

Nanostructured surfaces with novel and enhanced functionalities have been proposed for a wide spectrum of applications ranging from energy conversion and storage to membrane-based separation processes and catalysis [1–7]. This class of functional nanomaterials are expected to play a major role in the development of new technologies for moving toward sustainable production of energy and water in the coming decade [8-11]. Nanostructured surfaces with superhydrophilic or superhydrophobic properties have been extensively studied for (bio)fouling prevention, antifogging, and anti-icing [12-14], which are critical properties to improve performance, reduce energy consumption and operational costs of engineering systems based on membranes, electrodes, or catalyst surfaces. In particular, superhydrophobic surfaces with conical nanostructures with dimensions of the order of 10 nm and coated with octadecyltrichlorosilane (OTS) can produce large hydrodynamic slippage and repel water infiltration at very high hydrostatic pressures (e.g., up to 20 bar) [15], which makes them especially suitable for diverse separation and filtration processes where significant pressure heads need to be applied.

Transport processes in membranes and porous media are not only affected by surface wettability and hydrodynamic friction but also the development of surface charge and an electric double layer (EDL). Key phenomena such as selective transport, permeation, and adsorption of ions, nanoparticles, or microorganisms are governed by electrostatic and hydrodynamic effects within the EDL that are typically characterized by the surface zeta potential, its sign, magnitude, and variation with ionic concentration and pH [16–18]. While the surface charge and zeta potential of hydrophilic surfaces is fairly well understood and characterized [19-23], the mechanisms for surface charge formation and their interactions with hydrodynamic slip remain under active study for the case of hydrophobic interfaces [24-27]. To the best of our knowledge, this work is able to produce the first direct measurements of streaming potentials and zeta potentials for superhydrophobic nanostructured surfaces with large contact angles ( $\gtrsim 150^{\circ}$ ) large hydrodynamic slip length ( $\simeq$ 40 nm) owing to the synthesis of precise nanoscale structures over large area substrates.

The ability to fabricate large-area nanostructured surfaces with controllable and regular physical features is crucial for the development of future technical applications. Over the last two decades, microphase separation of block copolymers (BCPs) has been leveraged for nanofabrication techniques for large area substrates [28–31]. In this work, we follow the method based on BCP self-assembly reported in previous work [32] and refine the protocol

<sup>\*</sup> Corresponding author.

E-mail address: carlos.colosqui@stonybrook.edu (C.E. Colosqui).

in order to significantly reduce the fabrication time and prevent defects on slender structural features taller than  $\sim 100$  nm. We thus synthesize highly regular conical nanopillars with a fixed base radius and different heights over surface areas of the order of several square centimeters. The large-area nanostructured surfaces fabricated on silicon have a native oxide film and, in some cases, are passivated with OTS coating, which produces wetting behaviors ranging from superhydrophilic to superhydrophobic. The fabricated surfaces are suitable for conventional experimental techniques for determining zeta potentials via measurement of streaming potentials or streaming currents in electrokinetic flow through macroscale slit channels. Characterization of zeta potentials for the fabricated nanostructured surfaces are performed at pH 4 to 8 for aqueous electrolyte solutions of potassium chloride (KCl) with concentrations of 1 and 10 mM. The results and analysis provide useful guidelines for the future development of functional nanostructured materials for membrane-based filtration, energy conversion and storage, and selective adsorption and adhesion of ions, nanoparticles, or biomolecules.

#### 2. Materials and methods

The fabrication process based on BCP self assembly and plasma etching is illustrated in Fig. 1, the protocol employed in this work is a refined version of the one previously reported in Ref. [32]. The refined protocol significantly reduces the overall fabrication time by increasing the temperature in the thermal annealing steps. An additional etch step is included in order to synthesize tall and sharp conical nanopillars with heights larger than  $\geq 180$  nm.

Silicon wafers (type N, dopant P, orientation  $\langle 100 \rangle$ , University Wafer Inc.) are employed as substrates. The silicon substrates are first grafted (Fig. 1a) by spin-coating at 1500 rpm for 30 s a 1 wt% solution of PS-r-PMMA-OH random polymer brushes (molecular weight,  $M_w \simeq 9.2$  kg/mol, PS:PMMA = 61:39) in propylene glycol monomethyl ether acetate (PGMEA). Thermal annealing is then performed at 250 °C for 5 min, instead of 4 h at 200 °C as previously reported in Ref. [32]. Ungrafted polymer chains are removed by spin casting PGMEA at 3000 rpm for 30 s. The grafted silicon substrates induce the PMMA microdomains to orient perpendicular to the surface when the coating BCP films undergo microphase separation, which is crucial for the formation of a self-assembled pattern [31,38].

The employed BCP is polystyrene-block-methyl methacrylate (PS-b-PMMA) from Polymer Source. Inc. with molecular weights  $M_W=99$  kg/mol (PS:PMMA = 64:35, polydispersity PD=1.09). The PS-b-PMMA is mixed (1 wt%) in pure toluene and the solution is spin cast on the silicon wafer (Fig. 1a) at 2000 rpm for 30 s. Ordered PS and PMMA microdomains with cylindrical morphology self assemble in a nearly hexagonal lattice with spacing  $d\simeq 50$  nm (Fig. 1a and b) after performing thermal annealing at 250 °C for 20 min with nitrogen gas purging. The thermal annealing step described above requires significantly less time than the 12 h at 200 °C reported in Ref. [32].

A mask for subsequent reactive ion etching was formed by replication of the PMMA domain pattern in Al<sub>2</sub>O<sub>3</sub>, as described previously [32]. The substrate with the self-assembled BCP film is placed in an atomic-layer-deposition (ALD) chamber (Cambridge Nanotech Savannah S100) and subject to four sequential exposures to trimethylaluminum (TMA) for 100 s at 300 Torr, and water vapor for 100 s at 10 Torr and at a constant temperature of 85 °C (Fig. 1b). We employ four TMA deposition cycles, instead of the three cycles reported in Ref. [32], in order to increases the final thickness of the deposited aluminum oxide mask. Only the PMMA microdomains are transformed to aluminum oxide owing to the selective adsorption of the organoaluminium compound by PMMA. Etching with

oxygen plasma (March Plasma CS1701) at 20 W radio frequency (RF) power and 0.1 Torr is then performed for 300 s, which removes most of the organic materials and leaves aluminum oxide (Fig. 1b).

After the oxygen plasma etching, the silicon substrate with the deposited aluminum oxide mask (see SEM image in Fig. 1b) is placed in an Inductively Coupled Plasma (ICP) reactive ion etching system (Oxford Instrument Plasma Lab 100), which provides the ability to etch highly anisotropic features. An initial "breakthrough" step (Fig. 1c) is performed for 20 s (i.e., for twice as long as reported in Ref [32]) using BCl<sub>3</sub>:Cl<sub>2</sub> at a gas flow ratio 20:5 standard cubic centimeter per minute (sccm) with 100 W RF power, 0.01 Torr pressure, 800 W ICP power to etch through the aluminum and silicon oxides at the wafer surface in order to produce textures of uniform height. After this step, HBr, Cl<sub>2</sub>, and O<sub>2</sub> gases at 50:50:10 sccm ratio were employed at 100 W RF power, 0.01 Torr, and 250 W ICP power at room temperature (Fig. 1c) for 27, 60, and 120 s to obtain conical pillars of heights h = 60, 120, and 200 nm, respectively. After an additional 4s breakthrough time, a brief additional etching step using BCl<sub>3</sub>:Cl<sub>2</sub> (20:5 sccm) was performed for 12 s in order to remove aluminum oxide that is redeposited in significant amount during the HBr:Cl<sub>2</sub>:O<sub>2</sub> etching step and prevents further etching of tall conical nanostructures  $h \simeq 200$  nm. The remaining aluminum oxide mask is finally removed by dipping the samples in buffered (50:1) hydrofluoric (HF) acid solution for 50 s (Fig. 1c).

Some of the fabricated silicon surfaces are rendered superhydrophobic, as described in Ref. [32], by applying a monolayer of octadecyltrichlorosilane (OTS). These samples are first treated with piranha solution  $H_2SO_4$ : $H_2O_2$ =2:1 (volume ratio) and then immersion in a solution of OTS (Gelest inc.) and hexadecane (Sigma–Aldrich) for 1 h. Coating the surfaces with OTS prevents the slow formation of a thin silicon dioxide film when the samples are in contact with ambient oxygen and moisture or water at room temperature [33].

# 3. Results and discussion

The basic morphology of the synthesized nanostructures was studied via scanning electron microscopy (SEM) using a field emission microscope (Hitachi S-4800) operating at 10 kV. Well defined conical nanopillars of different height (Fig. 2a) are arranged in a nearly hexagonal lattice with a regular spacing  $d = 52 \pm 4$  nm, which corresponds well with the dimensions of etched masked produced by BCP self assembly (Fig. 1b). The SEM images (Fig. 2a) show a uniform nanopillar height  $h \simeq 60$ , 120, and 200 nm produced with different etching times. The average nanopillar radius measured from SEM images is  $r_t \simeq 7-8$  nm at the tip and  $r_h \simeq 12-20$ nm at the base (Fig. 2a). The measured tip radius and lattice spacing give the area fraction  $\varphi \simeq (2\pi/\sqrt{3})(r_t/d)^2 \simeq 0.07 - 0.09$  for direct contact between the wetting liquid and the top of the cones. A geometric parameter relevant to electroosmotic flow on hydrophilic surfaces is the full area ratio  $\Lambda = A(h)/A_0$  of the full wetted area (per unit cell)  $A(h) = 3\pi(r_b + r_t)\sqrt{h^2 + (rb - rt)^2} + A_0 - 3\pi r_b^2$  to the projected area  $A_0 = (3\sqrt{3}/2)d^2$ , which varies from 2.4 to 7.1 for the studied surfaces (see Fig. 2a).

Surface wettability. In order to characterize the wetting behavior of the synthesized surfaces, the advancing and receding contact angles  $\theta_A$  and  $\theta_R$ , respectively, were measured with an optical goniometer (DataPhysics OCA 15EC) using the sessile drop (needle-in) method with a water droplet of volume 3–4  $\mu$ L and adding/withdrawing rates of 0.2  $\mu$ L/s. The results reported in Fig. 2b reveal superhydrophilic behavior with very low advancing and receding contact angles  $\theta_A \simeq \theta_R < 10^\circ$  and negligible static hysteresis for the nanostructured silicon surfaces that were not passivated with OTS coating and form a thin (<1 nm) native oxide film while in contact with air at room temperature for up to 7 days [33]. It

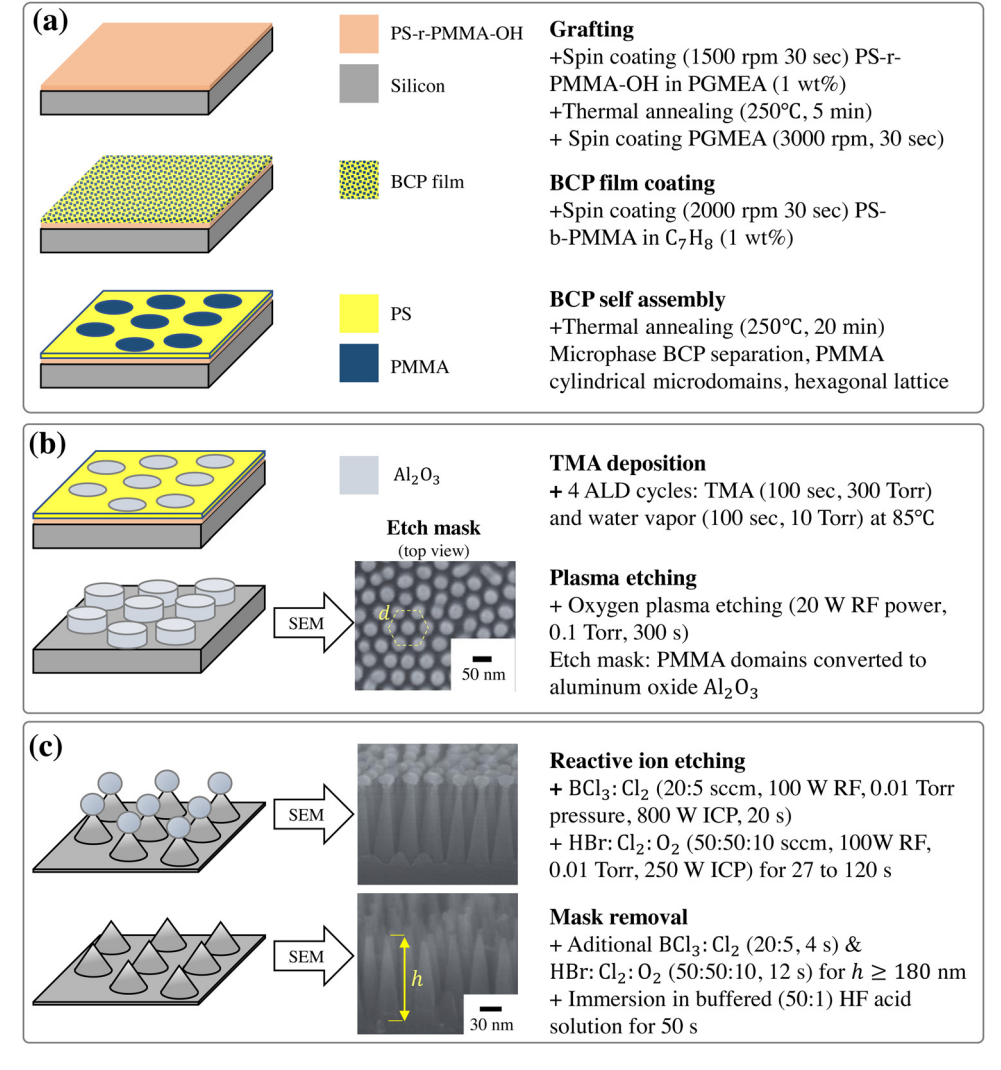


**Fig. 1.** Nanofabrication protocol based on BCP self-assembly. (a) BCP film coating and self-assembly on Si substrates. (b) TMA deposition and oxygen plasma etching. (c) Reactive ion etching and mask removal. SEM images (b-c) show the formation of conical nanostructures of height  $h \simeq 200$  nm arranged in a nearly hexagonal lattice with average spacing  $d \simeq 50$  nm.

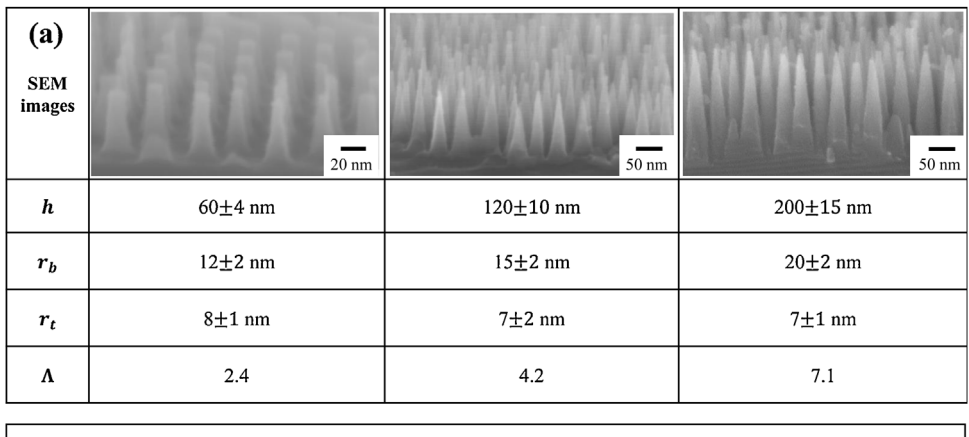
is worth noticing that the observed superhydrophilic behavior of the nanostructured silicon surfaces was not retained for the samples were in contact with aqueous electrolyte solutions for over 48 h. On the other hand, nanostructured surfaces treated with OTS exhibit robust superhydrophobic properties with very high advancing and contact angles ( $\theta_A \simeq \theta_R > 150^\circ$ ) and very low static hysteresis( $\theta_R - \theta_A \lesssim 5^\circ$ ). The same superhydrophobic behavior and static contact angles were observed both before and after the samples were put in contact with aqueous electrolyte solutions for 5 to 7 days.

Previous experimental measurements using atomic force microscopy (AFM) [34] reported slip lengths  $b=4\pm2$  nm for flat surfaces coated with a hydrophobic OTS film and large slip lengths  $b=44\pm4$  nm for the fabricated superhydrophobic OTS surfaces with conical nanopillars. The experimentally measured slip lengths are closely predicted by analytical expressions [35,36] derived by assuming perfect slip over the surface area fraction  $\varphi=7-9\%$  where the wetting liquid is in contact with the nanoscale vapor film trapped between surface features.

Zeta potential measurements. Zeta potential measurements for the fabricated surfaces were performed using the conventional streaming potential method [16] with an electrokinetic analyzer (Anton Paar SurPASS 3). In order to perform the electrokinetic flow measurements (Fig. 3a) two identical samples of each studied surface were cut precisely into rectangles of length L = 2 cm and width W=1 cm, and fit tightly in the measurement flow cell, which consists of a slit channel with adjustable height  $H = 105 \pm 5 \mu m$  across which the pressure head  $\Delta p$ , voltage difference  $\Delta V$ , and electrical resistance R are measured. Deionized (DI) water (LabChem) with very low conductivity (0.056 μS/cm) was used to prepare aqueous electrolyte solutions of KCl at 1 mM and 10 mM concentrations. The pH of the electrolyte solution is automatically controlled during the experiments via titration with a base (50 mM NaOH) and acid (50 mM HCl) solution. A volume of 100 mL of the KCl solution is flowed through the measurement cell with pressure heads  $\Delta p$  (0.2 to 0.6 bar). The pressure head is very slowly decreased over time (Fig. 3b), which ensures the observation of a linear relation between the measured streaming voltage and applied pressure (Fig. 3c) for  $\Delta V \rightarrow 0$ . Under such linear response conditions, for which  $\Delta V = (dV/dp) \times \Delta p$ , the zeta potential is given by

$$\zeta = \frac{dV}{dp} \times \frac{\mu}{\varepsilon_0 \varepsilon_R} \times \kappa, \tag{1}$$

where  $\mu \simeq 0.001$  Pa s is the viscosity of the aqueous electrolyte solution,  $\varepsilon_0$  and  $\varepsilon_R$  are the vacuum and relative permittivity, respectively, and  $\kappa = (1/R) \times (L/WH)$  is the electrical conductivity measured across the flow cell.



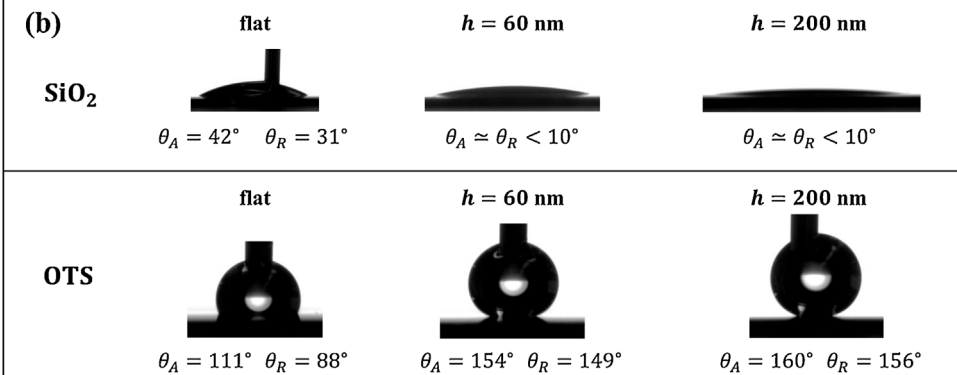


**Fig. 2.** Surface morphology and wetting properties of the fabricated nanostructured surfaces. (a) SEM images with measured height h, base radius  $r_b$ , tip radius  $r_t$ , and the calculated area ratio  $\Lambda$ . (b) Advancing contact angle  $\theta_A$  and receding contact angle  $\theta_R$  for flat and nanostructured surfaces with SiO<sub>2</sub> native films or OTS coatings. The nanostructured surfaces show macroscopic wetting properties ranging from superhydrophilic to superhydrophobic.

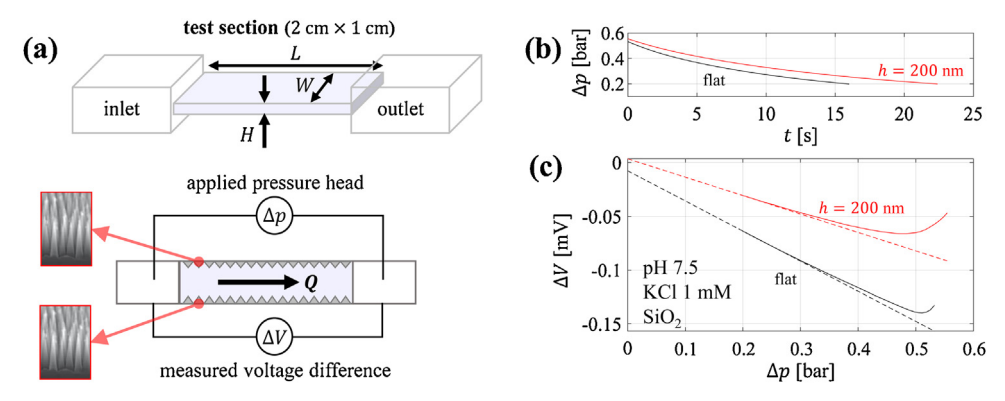


**Fig. 3.** Experimental configuration for zeta potential determination via streaming potential measurements. (a) Illustration of the test section of the electrokinetic analyzer (Anton Paar SurPASS 3) with the fabricated surface samples conforming a slit channel (L=2 cm, W=1 cm,  $H=105\pm5$   $\mu$ m). (b) Measured pressure head vs. time for a flat and nanostructured SiO<sub>2</sub> surface at pH 7.5 and 1 mM KCl as 100 mL of electrolyte solution flow through the test section illustrated in (a). (c) Measured voltage difference vs. pressure head for the conditions reported in panel (b). The voltage slope in the linear region where  $\Delta V/\Delta p \simeq$  const is employed to determine the zeta potential using Eq. (1).

The zeta potentials experimentally determined according to Eq. (1) are reported in Fig. 4 for the case of flat surfaces (i.e., without synthetic nanostructures) and the fabricated nanostructured surfaces described in Fig. 2, with and without hydrophobic OTS coating. The data reported for each studied surface correspond to four or five independent experiments repeated over a period of 2 to 5 days under controlled temperature conditions ( $T=25\pm3\,^{\circ}\text{C}$ ) at pH values between 4 and 8. To improve the reproducibility of the experimental conditions, the studied samples underwent four to seven rinse cycles with the employed electrolyte solution at each pH value prior to performing a single zeta potential measurement. The measurement cell was rinsed with 1 L of DI water after completing each experiment.

Both hydrophilic and hydrophobic surfaces with and without nanostructures reported negative zeta potential values with their magnitudes increasing with pH and with isoelectric points estimated at pH values between 2 and 3. The flat hydrophilic surfaces with a native SiO<sub>2</sub> film produced zeta potentials reaching about - 100 mV for 1 mM KCl (Fig. 4a) and -60 mV for 10 mM KCl (Fig. 4b) at pH 8, which is in close agreement with data reported by previous experimental studies [19–21]. The SiO<sub>2</sub> surfaces textured with nanocones of different height ranging from 60 to 200 nm exhibited similar zeta potentials within the range -20 to -50 mV for both 1 mM and 10 mM KCl (cf. Fig. 4a and b), which reveals that the fabricated nanostructures weaken the dependence of the zeta potential on the electrolyte concentration. The hydrophobic flat OTS surface

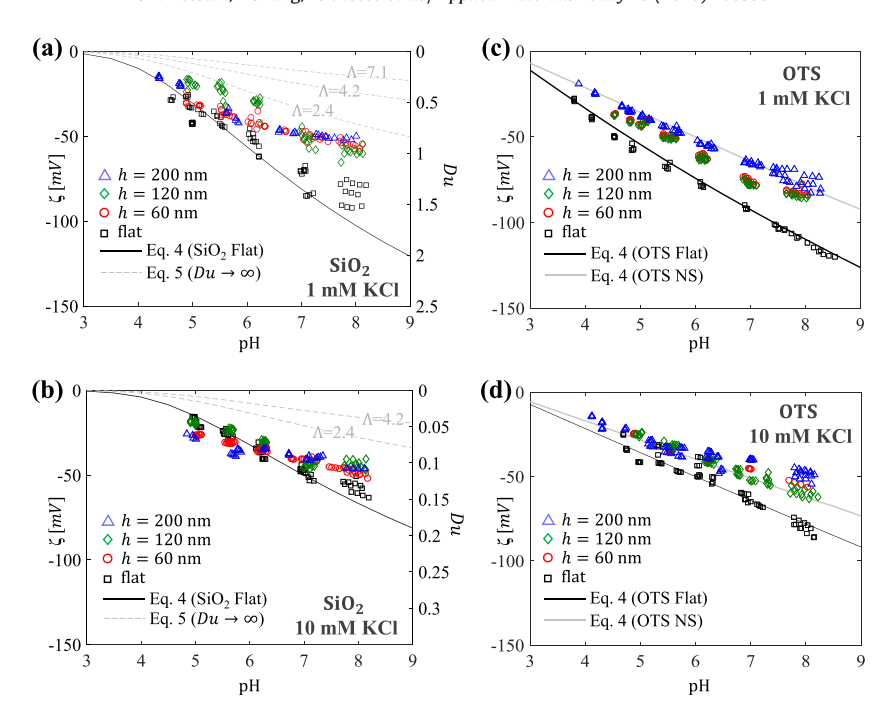


Fig. 4. Zeta potentials experimentally determined and analytical estimates for different pH and electrolyte concentrations 1 and 10 mM KCl. (a–b) Hydrophilic/superhydrophilic surfaces with a native  $SiO_2$  film. The Dukhin number defined for nanostructure hydrophilic surfaces (see text) is reported on the right vertical axes. (c–d) Hydrophobic/superhydrophobic surfaces with OTS coating. The slip length is b=4 nm for the flat OTS surfaces and b=44 nm for the nanostructured OTS surfaces. Markers indicate experimental results for the case of flat substrates and surfaces with conical nanostructures of different height h (see legend). Solid lines are predictions from Eq. 4 valid for  $Du \rightarrow 0$  and dashed lines are predictions from Eq. 5 valid for  $Du \rightarrow \infty$  with  $\Lambda = 2.4$ , 4.2, and 7.1 (see Fig. 2a).

produced the strongest zeta potentials, reaching  $-120\,$  mV for 1 mM KCl (cf. Fig. 4c) and  $-80\,$  mV for 10 mM KCl (cf. Fig. 4d) at pH 8, which is consistent with previous experimental measurements by a similar approach [37]. For both cases of surfaces with a native SiO<sub>2</sub> and coated OTS film the basic effect of the nanostructure was to reduce notably the zeta potential at the lowest studied electrolyte concentration (1 mM), for which the Debye length is about 10 nm and becomes comparable to the period between surface features. Despite the reductive effect of the surface nanostructure, the studied superhydrophobic surfaces attained significant zeta potentials ( $-20\,$  to  $-80\,$  mV) that are comparable to those of the flat hydrophilic surfaces.

Analytical predictions. The zeta potential measurements from our experiments are reasonably well accounted for by analytical predictions reported in Fig. 4 that are based on the interfacial configurations illustrated in Fig. 5a-b and a site-dissociation model relating the surface charge density  $\sigma$  and surface potential  $\psi_o$ . For all studied cases a constant specific capacitance  $C_s$  determines the diffuse-layer potential  $\psi_d = \psi_o - \sigma/C_s$  at the interface between the Stern and diffuse layers of the EDL (Fig. 5a and b). The employed site-dissociation model [38] assumes that the proton (H<sup>+</sup>) or hydronium  $(H_3O^+)$ , and hydroxide  $(OH^-)$  are the potential-determining cation and anion, for which the corresponding logarithmic dissociation constants are  $pK_{+}$  and  $pK_{-}$ , respectively. The surface charge model thus considers roughly the dissociation of silicon dioxide and silanol [39,40] for the studied hydrophilic surfaces (Fig. 5a) and the dissociation and selective adsorption of hydroxide and hydronium ions [41,42] in the case of superhydrophobic surfaces (Fig. 5b).

The charge density and surface electrostatic potential satisfy the relation [38]

$$\sigma = e\Gamma \frac{10^{(pH_0 - pK_-)} \times 2\sinh[e(\psi_N - \psi_0)/k_BT]}{1 + 10^{(pH_0 - pK_-)} \times 2\cosh[e(\psi_N - \psi_0)/k_BT]}$$
(2)

where e is the elementary charge,  $\Gamma$  is the total number of dissociation sites per unit area,  $pH_0 = (pK_+ + pK_-)/2$  is the pH value

for the isoelectric point, and  $\psi_N = -2.303(k_BT/e)(pH - pH_0)$  is the Nernst potential ( $k_B$  is the Boltzmann constant). Further assuming the total charge in the diffuse EDL neutralizes the surface charge (i.e., electroneutrality), the diffuse-layer potential must satisfy the Grahame equation

$$\psi_d = 2\frac{k_B T}{e} \operatorname{arcsinh}\left(\frac{\sigma e \ell_D}{2\varepsilon_o \varepsilon_R k_B T}\right) \tag{3}$$

where  $\ell_D = \sqrt{\varepsilon_o \varepsilon_R k_B T/2e^2 c N_A}$  is the Debye length determined by the electrolyte concentration c in molar ( $N_A$  is Avogadro's number). Solving the nonlinear system formed by Eqs. (2)–(3) gives the surface charge density and diffuse-layer potential, which is required to determine analytically the zeta potential.

Analytical solution of the nonlinear Poisson-Boltzmann equation for a slit channel of height  $H\gg\ell_D$ , width  $W\gg H$ , and length  $L\gg H$  gives the electrostatic potential  $\psi(y)=4 \operatorname{arctanh}[\tanh(e\psi_d/4k_BT)\exp(y/\ell_D-H/2\ell_D)]$  where y is the coordinate along the direction normal to the surface; this expression assumes  $\psi(0)=0$  and is only valid for  $H\gtrsim 5\ell_D$ . Assuming steady electroomostic flow  $u(y)=(\varepsilon_0\varepsilon_R\Delta V/\mu L)\times\left[\psi-\psi_d+b\frac{d\psi}{dy}(H/2)\right]$  with a constant liquid viscosity  $\mu$  and slip length b, the zeta potential is

$$\zeta = -\frac{\mu L}{\varepsilon_0 \varepsilon_R \Delta V} \times \frac{2}{H} \int_0^{H/2} u(y) dy = \psi_d + b \frac{\sigma}{\varepsilon_0 \varepsilon_R}, \tag{4}$$

in the case of flat slit channel of height  $H\gg\ell_D$ , given that  $(2/H)\int_0^{H/2}\psi(y)dy=\mathcal{O}(\ell_D/H)$ . For the case of hydrophilic surfaces with nanoscale structure or random roughness (Fig. 5a) the zeta potential

$$\zeta^* = \frac{\zeta}{\lambda(Du)} \tag{5}$$

is determined by a shape factor  $\lambda \ge 1$ , which for a given topography is a function of the Dukhin number [43]  $Du \simeq (4\ell_D/d)(1 +$ 

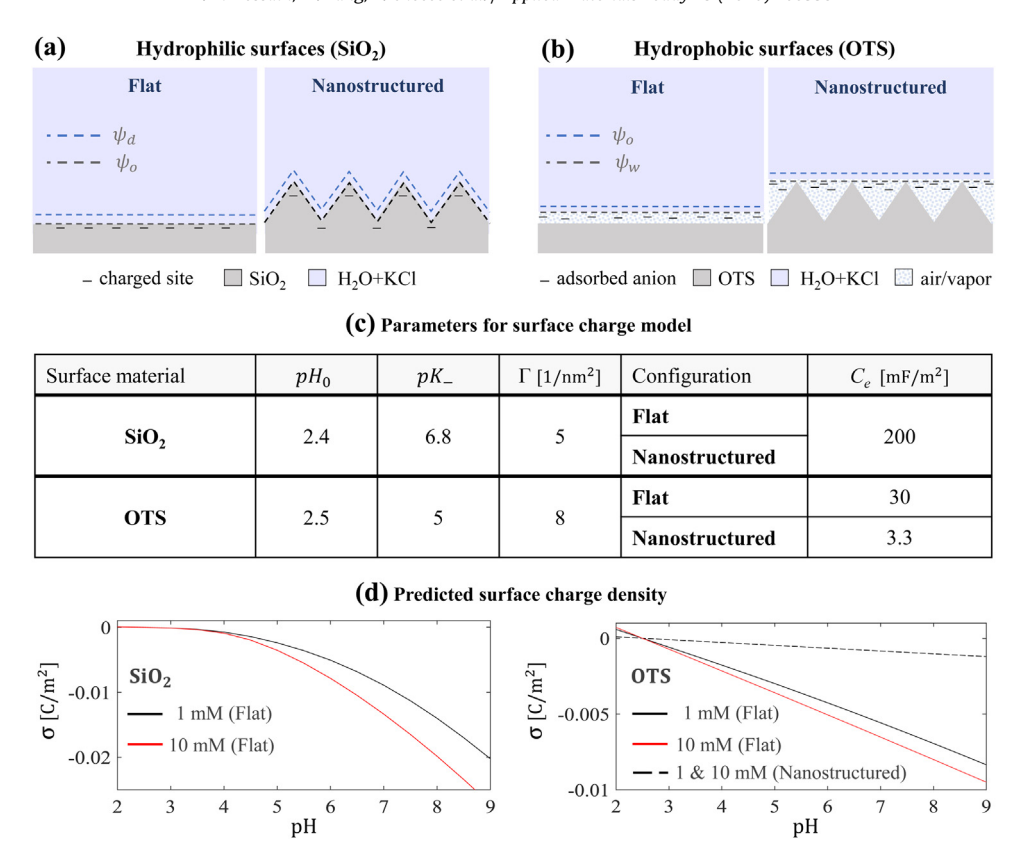


**Fig. 5.** Interfacial configurations, site-dissociation model, and surface charge density. (a) Hydrophilic surfaces (SiO<sub>2</sub>) are assumed to have the illustrated flat or "rough" interfacial configurations with charged sites at the water-oxide interface. (b) Hydrophobic surfaces (OTS) are assumed to have two flat interfacial configurations with preferential OH<sup>-</sup> dissociation and adsorption within the diffuse interfacial region between the vapor and water phases. (c) Model parameters for analytical estimates reported in Fig. 4 for the cases of SiO<sub>2</sub> surfaces and OTS surfaces in flat and nanostructured configuration. (d) Surface charge densities predicted by Eqs. (2)–(3) for electrolyte concentrations 1 and 10 mM KCl.

m)sinh<sup>2</sup>( $e\zeta/4k_BT$ ) where  $m=2\varepsilon_0\varepsilon_R(k_BT/e)^2/\mu D\simeq 0.6$  is the ratio of ionic electro-convection to diffusion for a potassium cation with diffusivity  $D = 1.6 \times 10^{-9} \text{ m}^2/\text{s}$ . There are two asymptotes for the shape factor in Eq. (5):  $\lambda = 1$  for  $Du \to 0$  [44]; and  $\lambda = \Lambda$  for  $Du \to \infty$ with the area ratio  $\Lambda = A(h)/A_0$  reported in Fig. 2a; which corresponds to the case of extremely large surface conductivity with the resulting electroosmotic flow suppression [45]. In the thin EDL limit  $\ell_D/d \to 0$  ( $d \lesssim h$ ), analytical solution of the 3D Laplace equation for the electrostatic potential [46,47] predicts that the electric field magnitude increases/decreases periodically at the nanostructure apex/base. Despite this effect, for  $Du \rightarrow 0$  the zeta potential for nanostructured surfaces in a slit channel is  $\zeta^* \simeq \zeta$  and can be predicted by Eq. (4), which is a property known as similitude of electroosmotic flows [44,48]. Indeed, experimental measurements for Du < 1 and for both flat and nanostructured SiO<sub>2</sub> (see Fig. 4ab) report similar zeta potentials that agree closely with analytical estimates from Eq. (4). Predictions from Eq. (5) with  $\lambda = \Lambda$  seem to bound the measurements for nanostructured SiO2 surfaces as  $Du \rightarrow \infty$  (Fig. 4a-b).

The analytical fits based on Eqs. (2)–(5) assume the interfacial configurations illustrated in Fig. 5a-b for hydrophilic and hydrophobic surfaces and employ the model parameters reported in Fig. 5c for the case of SiO<sub>2</sub> and OTS surfaces. While the model parameters employed for hydrophilic SiO<sub>2</sub> surfaces are consistent with values reported in the literature [39,40], for hydrophobic and OTS surfaces only the isoelectric point at  $pH_0 \sim 2.5$  has been reported previously [37,49,41]. For the hydrophobic OTS surfaces (cf. Fig. 5b) the chosen dissociation constant  $pK_- = 2pH_0$  corresponds to neglecting the contribution of hydronium cations to the surface charge, which is valid for the studied basic pHs [41],

and the dissociation-site density is determined as  $\Gamma = d_{H_2O}^{-2}$  where  $d_{H_2O} = 0.35$  nm corresponds to the effective diameter of a water molecule. The Stern capacitance dominates the zeta potential slope  $|d\zeta/dpH| \propto C_s$ , the low values required for analytical fits for the hydrophobic surfaces (cf. Fig. 5b-c) seem to indicate the presence of a Stern layer with the low permittivity of water vapor ( $\varepsilon_r \simeq 1$ ) and a thickness of 0.3 nm for the flat surfaces and about 2.5 nm for the nanostructured surfaces. Analytical predictions from Eq. (5) with  $\lambda \leq \Lambda$  cannot account for the experimental results for superhydrophobic nanostructured surfaces, which is consistent with the assumption of a nearly flat water-vapor interface for such surfaces.

### 4. Conclusions and outlook

This work contributes to better understanding and predicting the surface charge and zeta potential of large-area nanostructured surfaces with superhydrophilic and superhydrophobic properties that can be particularly suitable for the fabrication of more efficient separation micro/nanofluidic devices, filtration membranes, or high-performance electrodes. A key finding is that for large surface conductivities and  $Du \propto (\ell_D/d) \times \zeta^2 \gtrsim 1$  the synthesized nanostructures can substantially reduce the zeta potential magnitude and its dependence on the pH and electrolyte concentration. This is observed for the case of low electrolyte concentrations  $(\leq 1 \text{ mM})$  for which the Debye layer thickness is comparable to the nanoscale feature period. The zeta potentials for flat and nanostructure surfaces are similar in the case of large electrolyte concentrations ( ≥ 10 mM) for which the Debye layer becomes smaller than the synthesized surface features and  $Du \ll 1$  is very small, which is found to be consistent with the so-called similitude of electroosmotic flows with arbitrary geometry [44,48]. While the surface charge densities estimated for hydrophobic surfaces are much lower than estimated for the hydrophilic surfaces, the zeta potential magnitude of the hydrophobic surfaces is generally higher due to the presence of significant hydrodynamic slip, as predicted theoretically in previous works [24,50].

Our experimental results and analysis report the formation of significant negative surface charge on hydrophobic surfaces for pH  $\gtrsim$  3, which corroborates recent experimental studies by vibrational spectroscopy [41] and AFM [25,26,34]. Zeta potential measurements for flat and nanostructured OTS surfaces with nanoscale features of different height are accounted for by assuming a nearly flat interface and employing a much smaller capacitance than reported for hydrophilic SiO<sub>2</sub> surfaces. The smaller capacitance for the hydrophobic OTS surfaces can be attributed to a much smaller electrical permittivity in regions with net charge density that develop at hydrophobic water-vapor interfaces that are diffuse in nature [51,52].

The EDL model adopted in this work assumes a 1:1 symmetric electrolyte and no net charge present in the Stern layer having a single specific capacitance. Alternative models considering specifically adsorbed ions in the inner Stern layer with multiple specific capacitances [53,54], and/or considering the orientational order of water molecules and asymmetric ionic sizes [55,56] could be adopted, which will likely lead to a different parametrization than reported in this work (see Fig. 5c)). The simple EDL model and parameters employed in this work give reasonably good agreement with experimental measurements for a wide range of pH values (3 to 9) and electrolyte concentrations (1 to 10 mM) and can be thus applied to estimate the surface charge and zeta potential of the fabricated nanostructured surfaces under conditions that maximize their potential impact on technical applications. For example, for the fabricated superhydrophobic surface with nanocones of height h = 120 nm and a slit or pore height of H = 250 nm the hydrodynamic conductivity is twice as large as expected for conventional hydrophilic surfaces, which would reduce by 50% the pressure head and mechanical input power required to sustain the same flow rate through the system. For the same nanostructured surface and slit or pore geometry at an electrolyte concentration of 0.01 mM, the zeta potentials predicted analytically are less than 5% different from those reported in the present experiments. Under such conditions and for seawater with pH 7.5 to 8.5, maximum efficiencies between 40% and 55% are predicted for conversion of mechanical energy input into electrical power and between 30% to 40% for pumping fluid flow through applied voltage differences. The predicted performances of the fabricated nanostructured surfaces and the feasibility of their fabrication over large areas can lead to the development of much more efficient systems for molecular separations, energy conversion, or electroosmotic pumping and propulsion.

## Data availability

Raw and processed experimental data reported in this work are available upon request to the corresponding author.

### Acknowledgments

We gratefully acknowledge Benjamin Hsiao, Harold Walker, and Pejman Myavaghother for providing scientific and technical support to perform zeta potential measurements. We thank Esther Takeuchi, Amy Marschilok, and H. Scott Coombe for useful discussions on the technical impact and potential applications of the studied surfaces. The nanofabrication work was performed in user facilities at the Center for Functional Nanomaterials of Brookhaven National Laboratory under Contract No. DE ACO2 98CH10886. This

work is supported by the Office of Naval Research under award N00014-16-1-3178. A.A. was supported by the National Science FoundationCBET-1605809. C.C. was supported by the New York State Energy Research and Development Authority (NYSERDA, award 76890) and Department of Economic Development (DED, award 76890), which provided matching funds to the Center of Mesoscale Transport Properties, an EFRC from the U.S. Department of Energy, Office of Science (award DE-SC0012673). Opinions, findings, and conclusions in this work do not necessarily reflect those of the funding agencies.

#### References

- [1] M.J. Pitkethly, Nanomaterials-the driving force, Mater. Today 7 (12) (2004) 20–29.
- [2] Y.-G. Guo, J.-S. Hu, L.-J. Wan, Nanostructured materials for electrochemical energy conversion and storage devices, Adv. Mater. 20 (15) (2008) 2878–2887.
- [3] G.G. Wallace, J. Chen, A.J. Mozer, M. Forsyth, D.R. MacFarlane, C. Wang, Nanoelectrodes: energy conversion and storage, Mater. Today 12 (6) (2009) 20–27.
- [4] N.R. Shiju, V.V. Guliants, Recent developments in catalysis using nanostructured materials, Appl. Catal. A 356 (1) (2009) 1–17.
- [5] R. Narayan, Use of nanomaterials in water purification, Mater. Today 13 (6) (2010) 44–46.
- [6] Y. Han, Z. Xu, C. Gao, Ultrathin graphene nanofiltration membrane for water purification, Adv. Funct. Mater. 23 (29) (2013) 3693–3700.
- [7] P. Marchetti, M.F. Jimenez Solomon, G. Szekely, A.G. Livingston, Molecular separation with organic solvent nanofiltration: a critical review, Chem. Rev. 114 (21) (2014) 10735–10806.
- [8] M. Melchionna, P. Fornasiero, The role of ceria-based nanostructured materials in energy applications, Mater. Today 17 (7) (2014) 349–357.
- [9] H. Abe, J. Liu, K. Ariga, Catalytic nanoarchitectonics for environmentally compatible energy generation, Mater. Today 19 (1) (2016) 12–18.
- [10] T. Liu, J. Ding, Z. Su, G. Wei, Porous two-dimensional materials for energy applications: innovations and challenges, Mater. Today Energy 6 (2017) 79–95
- [11] R.J. Hamers, Nanomaterials and global sustainability, Acc. Chem. Res. 50 (3) (2017) 633–637.
- [12] J. Genzer, K. Efimenko, Recent developments in superhydrophobic surfaces and their relevance to marine fouling: a review, Biofouling 22 (5) (2006) 339–360
- [13] M.J. Kreder, J. Alvarenga, P. Kim, J. Aizenberg, Design of anti-icing surfaces: smooth, textured or slippery?, Nat. Rev. Mater. 1 (1) (2016) 15003.
- [14] M. Liu, S. Wang, L. Jiang, Nature-inspired superwettability systems, Nat. Rev. Mater. 2 (7) (2017) 17036.
- [15] A. Checco, B.M. Ocko, A. Rahman, C.T. Black, M. Tasinkevych, A. Giacomello, S. Dietrich, Collapse and reversibility of the superhydrophobic state on nanotextured surfaces, Phys. Rev. Lett. 112 (21) (2014) 216101.
- [16] R.J. Hunter, Zeta potential in colloid science: principles and applications, Vol. 2, Academic Press, 2013.
- [17] M. Elimelech, W.H. Chen, J.J. Waypa, Measuring the zeta (electrokinetic) potential of reverse osmosis membranes by a streaming potential analyzer, Desalination 95 (3) (1994) 269–286.
- [18] A. Al-Amoudi, P. Williams, S. Mandale, R.W. Lovitt, Cleaning results of new and fouled nanofiltration membrane characterized by zeta potential and permeability, Sep. Purif. Technol. 54 (2) (2007) 234–240.
- [19] L. Bousse, S. Mostarshed, B. Van Der Shoot, N. De Rooij, P. Gimmel, W. Göpel, Zeta potential measurements of ta2o5 and sio2 thin films, J. Colloid Interface Sci. 147 (1) (1991) 22–32.
- [20] P.J. Scales, F. Grieser, T.W. Healy, L.R. White, D.Y. Chan, Electrokinetics of the silica-solution interface: a flat plate streaming potential study, Langmuir 8 (3) (1992) 965–974.
- [21] B.J. Kirby, E.F. Hasselbrink Jr, Zeta potential of microfluidic substrates: 1. theory, experimental techniques, and effects on separations, Electrophoresis 25(2)(2004)187-202.
- [22] B.J. Kirby, E.F. Hasselbrink Jr., Zeta potential of microfluidic substrates: 2. data for polymers, Electrophoresis 25 (2) (2004) 203–213.
- [23] M. Lorenzetti, E. Gongadze, M. Kulkarni, I. Junkar, A. Iglič, Electrokinetic properties of tio 2 nanotubular surfaces, Nanoscale Res. Lett. 11 (1) (2016) 378.
- [24] L. Joly, C. Ybert, E. Trizac, L. Bocquet, Hydrodynamics within the electric double layer on slipping surfaces, Phys. Rev. Lett. 93 (25) (2004) 257805.
- [25] M.-C. Audry, A. Piednoir, P. Joseph, E. Charlaix, Amplification of electro-osmotic flows by wall slippage: direct measurements on ots-surfaces, Faraday discussions 146 (2010) 113–124.
- [26] Y. Pan, B. Bhushan, Role of surface charge on boundary slip in fluid flow, J. Colloid Interface Sci. 392 (2013) 117–121.
- [27] S. Maduar, A. Belyaev, V. Lobaskin, O. Vinogradova, Electrohydrodynamics near hydrophobic surfaces, Phys. Rev. Lett. 114 (11) (2015) 118301.
- [28] M. Park, C. Harrison, P.M. Chaikin, R.A. Register, D.H. Adamson, Block copolymer lithography: periodic arrays of ~ 1011 holes in 1 square centimeter, Science 276 (5317) (1997) 1401–1404.

- [29] T. Thurn-Albrecht, J. Schotter, G. Kästle, N. Emley, T. Shibauchi, L. Krusin-Elbaum, K. Guarini, C. Black, M. Tuominen, T. Russell, Ultrahigh-density nanowire arrays grown in self-assembled diblock copolymer templates, Science 290 (5499) (2000) 2126–2129.
- [30] J.K. Bosworth, M.Y. Paik, R. Ruiz, E.L. Schwartz, J.Q. Huang, A.W. Ko, D.-M. Smilgies, C.T. Black, C.K. Ober, Control of self-assembly of lithographically patternable block copolymer films, ACS Nano 2 (7) (2008) 1396–1402.
- [31] A. Rahman, P.W. Majewski, G. Doerk, C.T. Black, K.G. Yager, Non-native three-dimensional block copolymer morphologies, Nat. Commun. 7 (2016) 13988
- [32] A. Checco, A. Rahman, C.T. Black, Robust superhydrophobicity in large-area nanostructured surfaces defined by block-copolymer self assembly, Adv. Mater. 26 (6) (2014) 886–891.
- [33] M. Morita, T. Ohmi, E. Hasegawa, M. Kawakami, M. Ohwada, Growth of native oxide on a silicon surface, J. Appl. Phys. 68 (3) (1990) 1272–1281.
- [34] J. Heverhagen, M. Tasinkevych, A. Rahman, C.T. Black, A. Checco, Slip length enhancement in nanofluidic flow using nanotextured superhydrophobic surfaces, Adv. Mater. Interfaces 3 (17) (2016) 1600303.
- [35] C. Ybert, C. Barentin, C. Cottin-Bizonne, P. Joseph, L. Bocquet, Achieving large slip with superhydrophobic surfaces: Scaling laws for generic geometries, Phys. Fluids 19 (12) (2007) 123601.
- [36] A.M. Davis, E. Lauga, Hydrodynamic friction of fakir-like superhydrophobic surfaces, J. Fluid Mech. 661 (2010) 402–411.
- [37] J. Lützenkirchen, C. Richter, Zeta-potential measurements of ots-covered silica samples, Adsorption 19 (2-4) (2013) 217–224.
- [38] T.W. Healy, L.R. White, Ionizable surface group models of aqueous interfaces, Adv. Colloid Interface Sci. 9 (4) (1978) 303–345.
- [39] T. Hiemstra, W. Van Riemsdijk, G. Bolt, Multisite proton adsorption modeling at the solid/solution interface of (hydr) oxides: A new approach: I. model description and evaluation of intrinsic reaction constants, J. Colloid Interface Sci. 133 (1) (1989) 91–104.
- [40] S.H. Behrens, D.G. Grier, The charge of glass and silica surfaces, J. Chem. Phys. 115 (14) (2001) 6716–6721.
- [41] C. Tian, Y. Shen, Structure and charging of hydrophobic material/water interfaces studied by phase-sensitive sum-frequency vibrational spectroscopy, Proc. Natl. Acad. Sci. 106 (36) (2009) 15148–15153.
- [42] K. Roger, B. Cabane, Why are hydrophobic/water interfaces negatively charged? Angew. Chem. 51 (23) (2012) 5625–5628.

- [43] J. Lyklema, Fundamentals of interface and colloid science: Solid-Liquid Interfaces, Vol. 2, Elsevier, 1995.
- [44] E.B. Cummings, S. Griffiths, R. Nilson, P. Paul, Conditions for similitude between the fluid velocity and electric field in electroosmotic flow, Anal. Chem. 72 (11) (2000) 2526–2532.
- [45] R. Messinger, T. Squires, Suppression of electro-osmotic flow by surface roughness, Phys. Rev. Lett. 105 (14) (2010) 144503.
- [46] A. Weinstein, Generalized axially symmetric potential theory, Bull. Am. Math. Soc. 59 (1) (1953) 20–38.
- [47] E. Gongadze, D. Kabaso, S. Bauer, T. Slivnik, P. Schmuki, U. Van Rienen, A. Iglič, Adhesion of osteoblasts to a nanorough titanium implant surface, Int. J. Nanomed. 6 (2011) 1801.
- [48] J.G. Santiago, Comments on the conditions for similitude in electroosmotic flows, J. Colloid Interface Sci. 310 (2) (2007) 675–677.
- [49] T.W. Healy, D.W. Fuerstenau, The isoelectric point/point-of zero-charge of interfaces formed by aqueous solutions and nonpolar solids, liquids, and gases, J. Colloid Interface Sci. 309 (1) (2007) 183–188.
- [50] Y. Ren, D. Stein, Slip-enhanced electrokinetic energy conversion in nanofluidic channels, Nanotechnology 19 (19) (2008) 195707.
- [51] D.A. Doshi, E.B. Watkins, J.N. Israelachvili, J. Majewski, Reduced water density at hydrophobic surfaces: Effect of dissolved gases, Proc. Natl. Acad. Sci. 102 (27) (2005) 9458–9462.
- [52] D.J. Bonthuis, S. Gekle, R.R. Netz, Profile of the static permittivity tensor of water at interfaces: Consequences for capacitance, hydration interaction and ion adsorption, Langmuir 28(20)(2012)7679-7694.
- [53] D.C. Grahame, The electrical double layer and the theory of electrocapillarity, Chem. Rev. 41 (3) (1947) 441–501.
- [54] N. Sahai, D.A. Sverjensky, Evaluation of internally consistent parameters for the triple-layer model by the systematic analysis of oxide surface titration data, Geochim. Cosmochim. Acta 61 (14) (1997) 2801–2826.
- [55] B. JO'M, M. Devanathan, K. Muller, On the structure of charged interfaces, Proc. Royal Soc. A 274 (1963) 55–79.
- [56] E. Gongadze, A. Iglič, Asymmetric size of ions and orientational ordering of water dipoles in electric double layer model-an analytical mean-field approach, Electrochim. Acta 178 (2015) 541–545.